pISSN 1229-3008 eISSN 2287-6251
Progress in Superconductivity and Cryogenics
Vol.25, No.3, (2023), pp.38~42 https://doi.org/10.9714/psac.2023.25.3.038

Transient loss analysis of non-insulation high temperature superconducting coil using the field-based data profiling method

Hoon Jung[a], Yoon Seok Chae[a], June Hee Han[a], Ji Hyung Kim[b], Seung Hoon Lee[b], Ho Chan Kim[a], Young Soo Yoon[c], and Ho Min Kim[*, a]

[a] *Department of Electrical & Energy Engineering, Jeju National University, Jeju, 63243, Korea*
[b] *Electric Energy Research Center, Jeju National University, Jeju, 63243, Korea*
[c] *Department of Electrical Engineering, Shin Ansan University, Ansan, South Korea*

(Received 20 August 2023; revised or reviewed 28 September 2023; accepted 29 September 2023)

Abstract

The evaluation of no-insulation (NI) high-temperature superconducting (HTS) typically uses the lumped equivalent circuit (LEC) model. Constant parameters in the NI HTS LEC model accurately predict voltage and central magnetic field at currents below the critical current. However, it is difficult to find constant circuit parameters that simultaneously satisfy the measured voltage and magnetic field under overcurrent conditions. Recent research highlights changes in contact resistance during transient conditions, which may impact power loss estimation in NI HTS coils. Therefore, we confirm the influence of contact resistance changes on loss calculation in the transient state for NI HTS coil. To achieve this, we introduce a measurement data analysis method based on the LEC model and compare it with the LEC model using constant circuit parameters.

Keywords: *no-insulation, lumped equivalent circuit, variable contact resistance, transient loss*

1. INTRODUCTION

No-insulation (NI) high-temperature superconducting (HTS) coils are typically evaluated using lumped equivalent circuit (LEC) models [1-8]. Numerous studies have confirmed the effectiveness of these models in predicting the voltage and central magnetic field of the coil when operating currents are below the critical current [9-12]. However, achieving simultaneous satisfaction of the coil voltage and central magnetic field measured in a section above the critical current with a specific combination of circuit parameters can be challenging [13].

NI-HTS coils are often at risk of failure due to excessive current. To prevent this, stable control of the operating current of NI-HTS coils is necessary, with important parameters being inductance and contact resistance. These two parameters are crucial for determining the dynamic characteristics of the HTS coil and are typically required parameters for the current controller of converters [14].

To analyze interconnect lines, such as contact resistance and mutual inductance, the partial element equivalent circuit (PEEC) model is commonly utilized. This model allows for the analysis of current distribution by spatially dividing the model, enabling the extraction of an equivalent circuit model through analysis in both the time and frequency domains [15-18]. However, extracting parasitic components (resistance, inductance, and capacitance) is necessary for constructing a PEEC equivalent circuit. Various techniques for predicting contact resistance have been extensively researched [19-23]. Nonetheless, methods for fairly accurate prediction of contact resistance have not yet been established.

Recent research suggests that contact resistance is variable under transient conditions [24]. To ensure stable operation of the coil under excessive conditions, it is necessary to examine the changes in dynamic characteristic parameters of the coil during excessive situations. If the dynamic characteristic parameters vary depending on the operating conditions, there is a risk of malfunctioning the HTS coil due to controller errors. Furthermore, leakage current in the NI-HTS coil can cause losses in the contact resistance. Leakage current is prominent during overcurrent situations. Therefore, understanding the impact of contact resistance changes on leakage current-induced losses in the coil is crucial in excessive scenarios.

This study investigates the impact of contact resistance changes in the transient state on the loss calculation of the NI HTS coil. We present an overview of the LEC model for the NI HTS coil and introduce the field-based data profiling (FBDP) method, a measurement data analysis technique based on the LEC model of the NI HTS coil. We employ FBDP to analyze the transient loss in the NI HTS coil during over current, which is a typical test to evaluate the coil's behavior in the transient state. Additionally, we compare these results with the LEC model of the NI HTS coil with constant contact resistance, examining the impact of contact resistance changes on the transient loss of NI HTS coil.

* Corresponding author: hmkim@jejunu.ac.kr

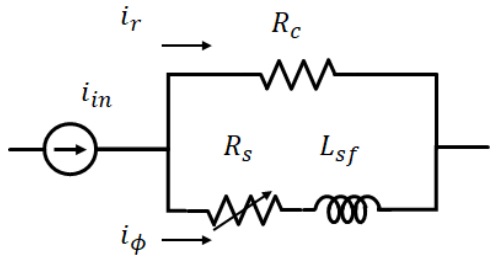

Fig. 1. Lumped-equivalent circuit for No-Insulation coil.

2. LUMPED-EQUIVALENT CIRCUIT MODEL AND DATA PROFILING METHOD

2.1. Lumped-equivalent circuit model of NI HTS coil

Fig. 1 shows the LEC simulation model of a typical NI HTS coil. In this model, R_s represents the azimuthal resistance, R_c represents the contact resistance, and L_{sf} represents the self-inductance. The voltage across the NI HTS coil is determined using Kirchhoff's voltage law and can be expressed as (1) [1-8]. In this equation, the left-hand side represents the voltage rise due to R_s in the superconducting layer, while the right-hand side represents the induced electromotive force caused by L_{sf}. Additionally, the voltage across the NI HTS coil is equal to the voltage across the radially parallel R_c.

The voltage across R_s is defined as (2). In this equation, I_c represents the critical current, which refers to the current at which the current versus voltage curve intersects the points of E_c = 1 μV/cm or E_c = 0.1 μV/cm. In the case of NI HTS coils, I_c should be determined based on the current flowing in the azimuthal direction, rather than the applied current.

Based on Kirchhoff's current law, the input current of the NI HTS coil can be expressed as (3), where i_ϕ represents the azimuthal direction current and i_r represents the leakage current. According to Ohm's law, R_s can be expressed as (4). When τ is the time constant, R_c can be calculated from (5).

$$v_o = V_c\left(\frac{i_\phi}{I_c}\right)^n + L_{sf}\frac{di_\phi}{dt} = R_c i_r \quad (1)$$

$$v_s = R_s i_\phi = V_c\left(\frac{i_\phi}{I_c}\right)^n \quad (2)$$

$$i_{in} = i_\phi + i_r \quad (3)$$

$$R_s = \frac{v_o}{i_\phi} \quad (4)$$

$$R_c = \frac{L_{sf}}{\tau} \quad (5)$$

2.2. Field-based data profiling analysis method

The FBDP is a back-calculation method using the LEC model of NI HTS coils. It assumes that i_ϕ produces a central magnetic flux density, B_{center}, which is linearly proportional to the magnetic coil constant κ. Previous research has employed this assumption to calculate i_ϕ [8, 9]. In this study, we have incorporated a procedure using the central difference method to calculate the inductive voltage in NI HTS coils. Consequently, variations of R_c could be calculated based on expressions of relation in the LEC model of NI HTS coil. The detailed procedure of FBDP is as follows:

STEP.1. Calculate i_ϕ by dividing the B_{center} measured from the experiment by κ [8, 9].

STEP.2. Calculate i_r by subtracting i_Φ from i_{in} from (3).

STEP.3. The induced electromotive force is calculated as follows by the central difference method as follow:

$$L_{sf}\frac{di_\phi}{dt} = \frac{L_{sf}}{2T_s}\left[i_\phi(\text{i+1}) - i_\phi(\text{i-1})\right], \quad (6)$$

where T_s represents the sampling time interval of the measured data, and i means the i-th data of the measured data.

STEP.4. Calculate v_s by subtracting the induced electromotive force from v_o using (1).

STEP.5. Calculate R_c by dividing i_r by v_o.

STEP.6. Assuming *n-value*, calculate I_c using (2); The HTS wire used for the tested NI HTS coil, SuNAM's GdBCO, wire with a width of 4.1 mm and a thickness of 140 μm, had an I_c and *n-value* of 216 A and 40, respectively, under self-field conditions at a liquid nitrogen (LN_2) cooling temperature of 77 K. In this study, an n-value of 40 was assumed, consistent with the *n-value* of the HTS wire used for the tested NI HTS coil.

The instantaneous power loss of the NI HTS coil is calculated as shown in (7). The left side of the equation represents the superconducting layer loss, while the right side represents the contact resistance loss.

$$P_{total} = v_s i_\phi + R_c i_r^2 \quad (7)$$

3. ANALYSIS RESULTS OF OVER-CURRENT EPXRIMENT

The over-current experiment was conducted with a final input current of 132 A, a ramp rate of 0.5 A/s, and a hold time of 60 seconds. The input current was set to 1.3 times I_c. Table I presents the detailed specifications of the tested NI HTS coil. A total of 31 turns were wound on a circular bobbin with a diameter of 80 mm, applying a winding tension of 3 kgf. The HTS wire used in the coil had a total length of 811 cm, which is important for determining the terminal tap voltage required for calculating the critical current. The self-inductance of this coil was measured to

TABLE I
SPECIFICATION OF NI HTS COIL

Parameter	
Number of turns	31
Insulation	None
Inner diameter/outer diameter	80 mm/ 88.68 mm
Winding tension	3 kgf
Total length of HTS wire	811 cm
L_{sf}	141 μH
τ	12 s
R_c	14.50 μΩ
κ	460 μT/A
I_c @ 77 K, self-field	100 A

be 141 μH, corresponding to a time constant of 12 seconds. Additionally, the contact resistance was calculated to be 14.5 μΩ using the measured time constant of 12 seconds. Moreover, the coil exhibited a critical current of approximately 100 A. Lastly, the coil constant, defined as the center magnetic field per ampere, was calculated to be 460 μT/A.

3.1. Comparison with Experimental and LEC Simulation Results

Fig. 2(a) presented a comparison of voltage in the NI HTS coil during the overcurrent test, showing that at an operating current of 132 A, the measured v_o was 901 μV, while the LEC simulation yielded a calculated value of 47 μV. The experimental v_o was 1.9 times higher than the simulation.

Fig. 2(b) compared B_{center}, with a measured value of 46 mT in the experiment and a calculated value of 45 mT in the LEC simulation. The LEC simulation estimated B_{center} by multiplying κ of 460 μT/A with i_ϕ. The measured and simulated B_{center} values were nearly identical.

3.2. Comparison with Experimental and LEC Simulation Results

Fig. 3(a) illustrated the variation of the i_r to i_Φ ratio in the over-current test. At operating current of 132 A, both the FBDP analysis and LEC simulation demonstrate a ratio of 0.33, indicating strong agreement. This agreement confirms that i_Φ and i_r, calculated using both methods, were identical at the given operating current. As a result, assuming κ is constant, the calculation of i_Φ in both the LEC simulation and FBDP leaded to the same B_{center} value.

Fig. 3(b) illustrated the variation of R_c and R_s in the over-current test. In the LEC simulation, R_c remained constant at 14.50 μΩ. However, in the FBDP analysis, R_c changed from 14.50 μΩ to 27.86 μΩ over time. Both LEC simulation and FBDP analysis resulted in an R_s value of 0 Ω when the operating current was increased and decreased at a rate of 0.5 A/s. Under the over-current condition with an operating current of 132 A, the LEC simulation showed R_s changing from 0 Ω to 4.79 μΩ, while the FBDP analysis showed R_s changing from 0 Ω to 9.18 μΩ. Consequently, the FBDP-calculated R_c and R_s were 1.9 times larger than the values obtained from the LEC simulation under the over-current condition.

Both FBDP analysis and LEC simulation yielded a consistent i_r to i_Φ ratio of 0.33 at an operating current of 132 A under overcurrent conditions. However, there was a notable distinction in the calculated R_c and R_s values. The FBDP analysis produced R_c and R_s values that were 1.9 times larger compared to the values obtained from the LEC simulation. This dissimilarity was further supported by the measurement of v_o in Fig. 2(a), which was 1.9 times larger (901 μV) than the LEC simulation value of 473 μV, despite similar i_r values in both methods. Because the v_o was calculated by multiplying R_c with i_r. Consequently, the main factor contributing to the difference between FBDP and LEC simulation results was the variation of R_c.

Fig. 4 shows the comparison of I_c obtained through both the FBDP and the LEC simulation methods. In the FBDP method, I_c was calculated using (9) based on the measured data. On the other hand, in the LEC simulation method, I_c is a constant value of 100 A derived from the I_c measurement test. While maintaining the operating current at 132 A, the FBDP calculation shows that I_c is 98 A, which is slightly smaller than the I_c value of 100 A used in the LEC simulation. This analysis suggests that the difference in R_s, as shown in Fig. 3(b), can be attributed to the difference in I_c between the two methods.

Fig. 5 compares the instantaneous power losses in the NI

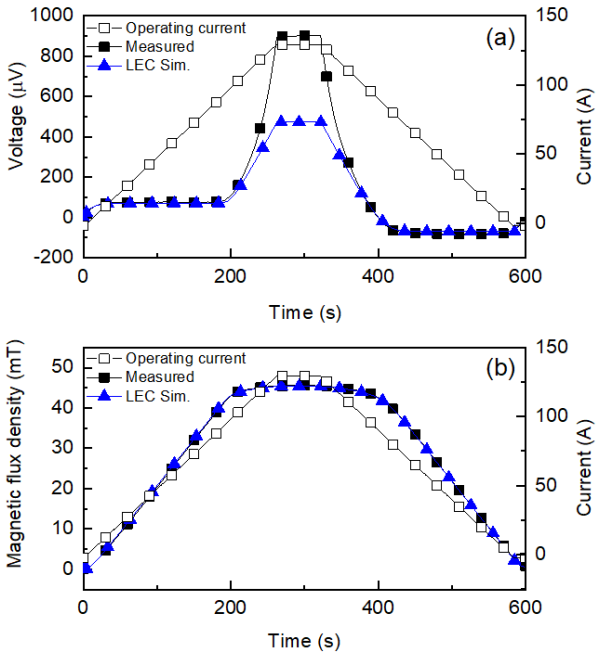

Fig. 2. Comparisons of (a) v_o, and (b) B_{center} in the NI HTS coil between experiment and LEC simulation during over current test.

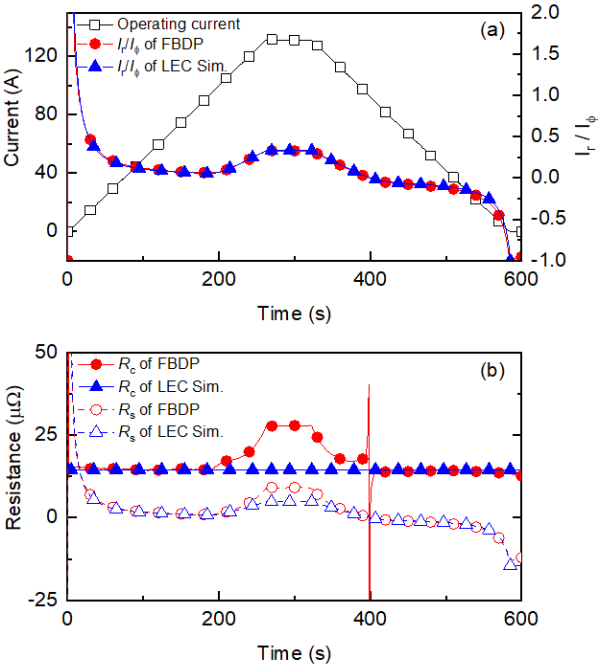

Fig. 3. Comparisons of (a) i_r/i_Φ, and (b) R_c and R_s in the NI HTS coil between FBDP and LEC simulation during over current test.

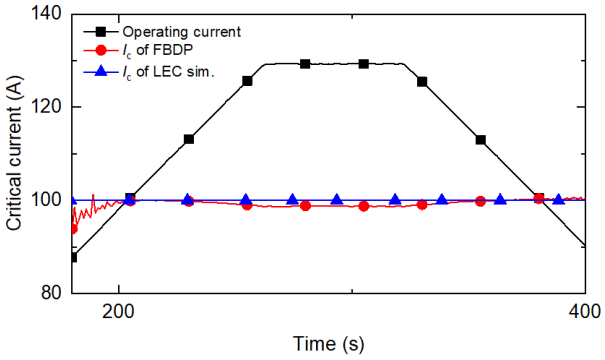

Fig. 4. Comparison of critical current in the NI HTS coil between FBDP and LEC simulation during over current test.

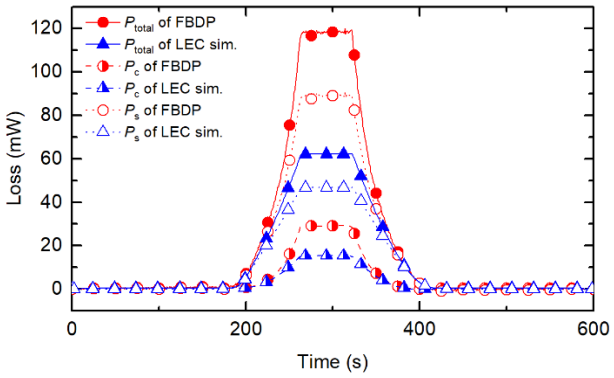

Fig. 5. Comparison of instantaneous power losses in the NI HTS coil between FBDP and LEC simulation during over current test.

HTS coil between FBDP and LEC simulation. We estimated the losses in the NI HTS coil under an operating current of 132 A. The contact resistance losses were calculated to be 29 mW and 15 mW for the FBDP and LEC simulations, respectively. Additionally, the azimuthal direction resistance losses were 88 mW and 46 mW for the FBDP and LEC simulations, respectively. Overall, the total power losses reached 117 mW and 62 mW in the FBDP and LEC simulations, respectively. As a result, the total power loss in the FBDP simulation was 1.9 times higher than in the LEC simulation.

4. CONCLUSION

In this paper, the impact of contact resistance changes during the transient state on the loss calculation of the NI HTS coil was investigated. This was done by analyzing experimental data obtained from an overcurrent test at 132 A, which corresponds to 1.3 times critical current. The FDBP method was employed for this analysis. Moreover, the FDBP analysis results were compared with those of the LEC model, which utilizes constant circuit parameters. Simulations of the NI HTS LEC model, which assumed constant circuit parameters, showed good agreement between the calculated and measured center magnetic flux density of NI HTS coil values. However, the calculated voltage of NI HTS coil was found to be lower than the measured value. The reason why the measured center magnetic flux density of NI HTS coil matches well with the simulated center magnetic flux density of NI HTS coil in the NI HTS LEC model could be because the real azimuthal direction current and radial leakage current, obtained from the FBDP analysis, agree with the simulated results under the assumption of a constant magnetic coil constant. However, when the same current flows through each layer, the FBDP analysis shows that azimuthal direction resistance and contact resistance increase in the experimental results. This might be the reason why the measured voltage of NI HTS coil ends up being greater than the simulated voltage of NI HTS coil in the experiment. As a result, the total instantaneous power loss in the FBDP analysis is calculated to be higher than that in the LEC simulation. The FBDP analysis method is expected to more accurately evaluate the loss of non-insulated high-temperature superconducting coils by considering the effect of contact resistance change in the transient state.

ACKNOWLEDGMENT

This research was supported by National R&D Programs through the National Research Foundation of Korea (NRF) funded by Ministry of Science and ICT. (Nos. 2021R1C1C2003235 and 2022M3I9A1072846)

REFERENCES

[1] S. Hahn, D. K. Park, J. Bascunan and Y. Iwasa, "HTS Pancake Coils Without Turn-to-Turn Insulation," *IEEE Trans. Appl. Supercond.*, vol. 21, no. 3, pp. 1592-1595, 2011.

[2] S. Hahn, D. K. Park, J. Voccio, J. Bascuñán and Y. Iwasa, "No-Insulation (NI) HTS Inserts for >1 GHz LTS/HTS NMR Magnets," *IEEE Trans. Appl. Supercond.*, vol. 22, no. 3, pp. 4302405-4302405, 2012.

[3] S. Hahn, et al., "A 78-mm/7-T Multi-Width No-Insulation ReBCO Magnet: Key Concept and Magnet Design," *IEEE Trans. Appl. Supercond*., vol. 24, no. 3, pp. 1-5, 2014.

[4] S. Hahn, et al., "No-insulation multi-width winding technique for high temperature superconducting magnet," *Appl. Phys Lett*, vol. 103, no. 17, 2013.

[5] Liu. L, et al., "Transient Electrical Characteristics of No-Insulation REBCO Coil Impregnated With GaInSn Liquid Metal," *IEEE Trans. Appl. Supercond.*, vol. 32, no. 9, pp. 1-6, 2022.

[6] J. Kim, et al., "Self-Protection Characteristic Comparison Between No-Insulation, Metal-as-Insulation, and Surface-Shunted-Metal-as-Insulation REBCO Coils," *IEEE Trans. Appl. Supercond*., vol. 33, no. 5, pp. 1-5, 2023.

[7] J. Kim, et al., "Effect of Resistive Metal Cladding of HTS Tape on the Characteristic of No-Insulation Coil," *IEEE Trans. Appl. Supercond*, vol. 26, no. 4, pp. 1-6, 2016.

[8] Y. Li, et al., "Feasibility Study of the Impregnation of a No-Insulation HTS Coil Using Solder," *IEEE Trans. Appl. Supercond*., vol. 28, no. 1, pp. 1-5, 2018.

[9] J. B. Song, S. Hahn, "Leak Current correction for critical current measurement of no-insulation HTS coil," *Prog. Supercond. Cryog.*, vol. 19, no. 2, pp. 48-52, 2017.

[10] B. Cho, J. Lee, "Numerical analysis on the critical current evaluation and the correction of no-insulation HTS coil." *Prog Supercond Cryog*, vol. 25, no. 1, pp. 16-20, 2023.

[11] M. Cho, et al., "Combined Circuit Model to Simulate Post-Quench Behaviors of No-Insulation HTS Coil," *IEEE Trans. Appl. Supercond*, vol. 29, no. 5, pp. 1-5, 2019.

[12] U. Bong, et al., "Compensation of NI Behaviors in Synchronous Motors With NI HTS Field Winding Using Harmonic Current Injection," *IEEE Trans. Appl. Supercond*, vol. 33, no. 5, pp. 1-5, 2023.

[13] C. Im, et al., "Mesh Dependency on a Partial Element Equivalent Circuit Model for an NI HTS Coil," *IEEE Trans. Appl. Supercond.*, vol. 31, no. 5, pp. 1-5, 2021.

[14] NI-REBCO Team, and S. Hahn. "Achievements, Progress, and Issus in No-Insulation HTS Coils," *13th European Conference on Applied Superconductivity (EUCAS2017)*, Geneva, Switzerland, 2017.

[15] B. Pu, J. S. Lee, W. S. Nah. "Electrical parameter extraction of high-performance package using PEEC method," *J. Korean Inst. Electromagn*, vol. 11, no. 1, pp. 62-69, 2011.

[16] S. An, et al., "Fast Distributed Simulation of "Defect-Irrelevant" Behaviors of No-Insulation HTS Coil," *IEEE Trans. Appl. Supercond*., vol. 31, no. 5, pp. 1-5, 2021.

[17] C. Genot, T. Lécrevisse, P. Fazilleau and P. Tixador, "Transient Behavior of a REBCO No-Insulation or Metal-as-Insulation Multi-Pancake Coil Using a Partial Element Equivalent Circuit Model," *IEEE Trans. Appl. Supercond.*, vol. 32, no. 6, pp. 1-5, 2022.

[18] J. T. Lee, et al., "Experimental and Equivalent Circuit Analysis Approach to Estimate Contact Resistances on Different Sections in a D-Shaped NI HTS Coil," *IEEE Trans. Appl. Supercond.*, vol. 33, no. 5, pp. 1-5, 2023.

[19] J. Bang, et al., "Experiment and Analysis on Temperature-Dependent Electric Contact Resistivity of an NI HTS Coil," *IEEE Trans. Appl. Supercond.*, vol. 33, no. 5, pp. 1-5, 2023.

[20] M. H. Sohn, K. Sim, B. Eom, H. S Ha, H. Y. Kim, K. Seong, "Controllability of the Contact Resistance of 2G HTS Coil With Metal Insulation," *IEEE Trans. Appl. Supercond.*, vol. 28, no. 3, pp. 1-5, 2018.

[21] T. S. Lee, et al., "The effects of co-wound Kapton, stainless steel and copper, in comparison with no insulation, on the time constant and stability of GdBCO pancake coils," *Supercond. Sci. Techno.*, vol. 27, no. 6, pp.1-8, 2014.

[22] T. Kurauchi, S. Noguchi, "Unbalanced radial current flow simulation of no-insulation REBCO pancake coils during normal state transition." *Supercond. Sci. Technol.*, vol. 33, no. 10, 2020.

[23] S. Xue, M. Sumption, E. Collings "YBCO coated conductor interlayer electrical contact resistance measured from 77 K to 4 K under applied pressures up to 9.4 MPa." *IEEE Trans. Appl. Supercond*., vol. 31, no. 5, pp. 1-5, 2021.

[24] J. Chen et al., "Investigation and analysis of turn-to-turn contact resistance of a no-insulation YBCO pancake coil under time-varying," *Phys. C: Supercond. Appl.*, vol. 576, 2020.

[25] IEC 61788-26:2020 "Superconductivity – Part 26: Critical current measurement – DC critical current of RE-Ba-Cu-O composite superconductors," 2020.